Biophysical Journal, Volume *113*

Supplemental Information

High Tensile Strength of Engineered β-Solenoid Fibrils via Sonication and Pulling

Zeyu Peng, Amanda S. Parker, Maria D.R. Peralta, Krishnakumar M. Ravikumar, Daniel L. Cox, and Michael D. Toney

Supplementary Information for "High Tensile Strength of Engineered Beta Solenoid Fibrils Determined in Sonication Experiments and Pulling Simulations"

Zeyu Peng[1], Amanda S. Parker[2], Maria D.R. Peralta[1], Krishnakumar M. Ravikumar[2], Daniel L. Cox[2], Michael D. Toney[1]

[1]*Department of Chemistry, University of California, Davis, California, USA,* [2]*Department of Physics, University of California, Davis, California*

1 Protein sequences

Here we report the sequences of the proteins used in the study, the antifreeze protein of the *Rhagium inquisitor* beetle, RiAFP, and the antifreeze protein of the spruce budworm, SBAFP.

MAHHHHHHSGS	
GSRAEARGEAMAEGHSRGCA	ASRAEARGEAMAEGHSRGCA
TSHANATGHADARSMSEGNA	TSHANATGHADARSMSEGNA
EAYTEAKGTAMATSEASGEA	EAYTEAKGTAMATSEASGEA
RAQTNADGRAHSSSRTHGRA	RAQTNADGRAHSSSRTHGRA
DSTASAKGEAMAEGTSDGDA	DSTASAKGEAMAEGTSDGDA
KSYASADGNACAKSMSTGHA	KSYASADGNACAKSMSTGHA
DATTNAHGTAMADSNAIGEA	DATTNAHGTAMADSNAIGEA
RAETRAEGRAESSSDTDGC	RAETRAEGRAESSSDTDGC

Table 1: Sequences of RiAFP used in experiment (left) and simulation (right). The initial tag of 12 amino acids (first row) of experimental sequence (left) was exluded in MD simulations. The rows represent individual turns of the beta-solenoid. The termination sequence does not affect the beta sheet structure crucial for the tensile strength or Young's modulus of the protein.

M	
ASRITNSQIVKSEAT	ASRITNSQIVKSEAT
NSDINNSQLVDSIST	NSDINNSQLVDSIST
RSQYSDANVKKSVTT	RSQYSDANVKKSVTT
DSNIDKSQVYLTTST	DSNIDKSQVYLTTST
GSQYNGIYIRSSDTT	GSQYNGIYIRSSDTT
GSEISGSSISTSRIT	GSEISGSSISTSRIT
NSRITNSQIVKSEAT	NSRITNSQIVKSEAT
NSDINNSQLVDSIST	NSDINNSQLVDSIST
RSQYSDANVKKSVTT	RSQYSDANVKKSVTT
DSNIDKSQVYLTTST	DSNIDKSQVYLTTST
GSQYNGIYIRSSDTT	GSQYNGIYIRSSDTT
GSEISGSSISTSRIT	GSEISGSSISTSRIT

Table 2: Sequences of SBAFP used in experiment (left) and simulation (right). The initial tag of one amino acid (first row) of experimental sequence (left) was exluded in MD simulations. The rows represent individual turns of the beta-solenoid. The termination sequence does not affect the beta sheet structure crucial for the tensile strength or Young's modulus of the protein.

2 Interface structure of oxidized RiAFP fibrils

Here we include an image of the interface between two RiAFP proteins when in the non-reduced state. See Fig. 1.

3 Cross-sectional area

The average cross-sectional area of the protein was calculated by treating each atom as a van der Waals' sphere and projecting these spheres on a planar surface perpendicular to the helical axis of the protein. A planar-grid of about 0.3 Ang was used to measure the area of this projection. This was done by sampling the grid. The ratio of points that fell inside the projection to total grid points, multiplied by the area of the grid, was taken as the area of the projection. This was repeated for each turn, and the average of all turns was taken as the cross-sectional area of the protein.

An illustration of this is shown in Fig. 3, where on the left is shown the atoms of one turn of each protein, represented as van der Waal's spheres, and on the right are those spheres projected onto a 2D grid and then sampled to produce an estimate of the cross-sectional area and perimeter or circumference.

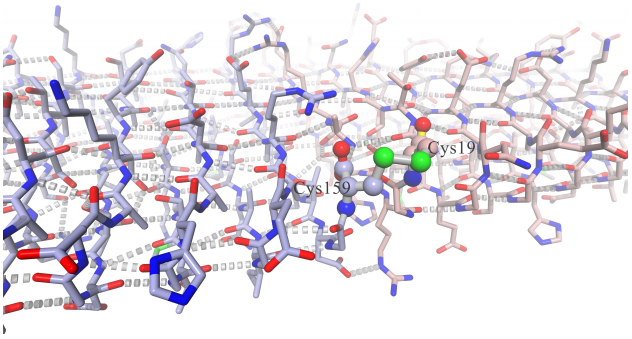

Figure 1: Model of the fibril interface between two RiAFP proteins in the nonreduced (oxidized) state. The design includes a single disulfide bond between a cysteine near the C-terminus (Cys159) and one near the N-terminus (Cys19). The backbone hydrogen bonding structure is also shown. This picture was created in YASARA [5].

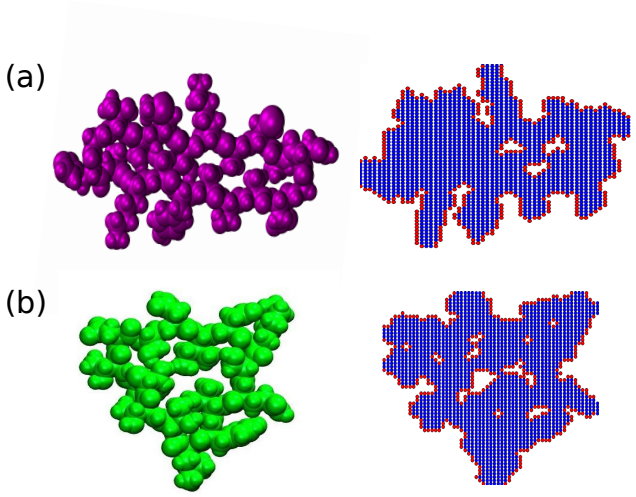

Figure 2: On the left, renderings of one turn of (a) RiAFP and (b) SBAFP, using van der Waal's spheres are shown. (Images created using VMD.) On the right, a grid sampling representation of the projection of these areas are shown in blue, as well as the circumferences in red.

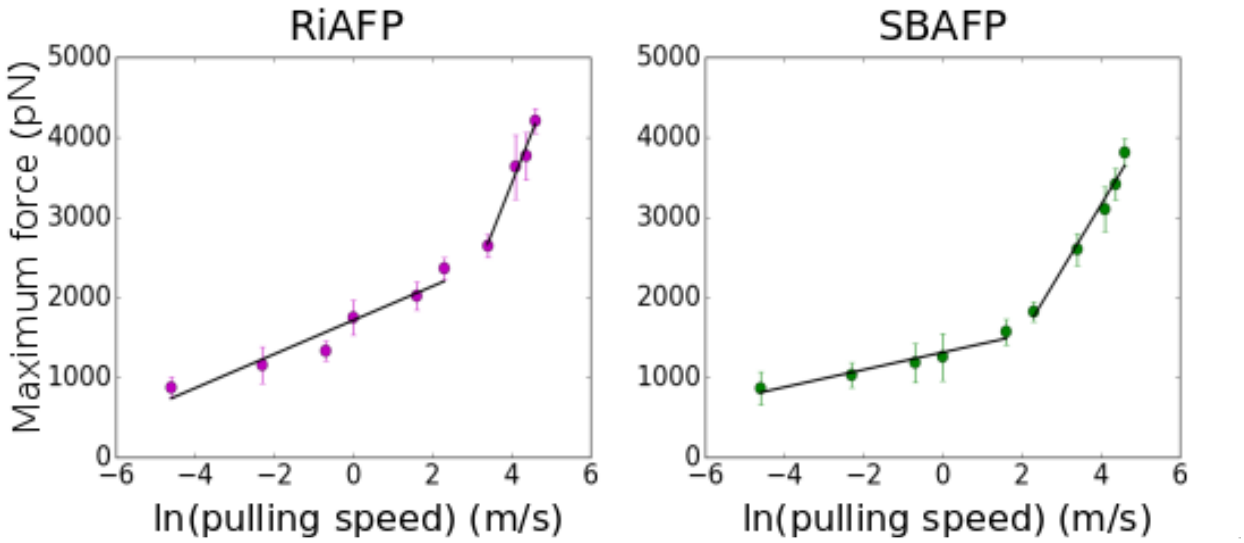

Figure 3: The average and standard deviation of the maximum force at each speed is shown for the RiAFP (purple) and SBAFP (green). Note that as with UTS, we observe two linear regimes, to which we fit two lines. Unlike the UTS, the rupture force values for RiAFP are generally larger than for SBAFP.

4 Displacement at maximum force and pulling speed

In addition to investigating the dependence of maximum force on pulling speed, the average breaking displacement at each speed was studied. Note that for the simulations results of Fig. 7 of the main article, the displacement at maximum force is nearly the same for both proteins (in the shown examples around 0.2 nm), which is true at all pulling speeds. Like the maximum force, the displacement also increased linearly with increasing pulling speed. Though the error bars are larger for the displacement values than for the forces, there does not seem to be two linear regimes when plotted against the natural log of the speeds, as there are for the forces.

5 Maximum forces and pulling speed

The ultimate tensile strength (UTS) is calculated by finding the breaking force, which we identify as the maximum force over the constant-speed pulling simulation, divided by the cross-sectional area. In Fig. 3, we plot the breaking forces alone as a function of the natural log of the pulling speed.

6 Hydrogen bonds and displacement

During a constant-speed pulling simulation, the force on the protein increases until the hydrogen bond network maintaining the secondary structure is broken. This can be observed in the trajectories (visualized in software such as VMD [4]) and in an analysis of the numbers of hydrogen bonds during the simulation.

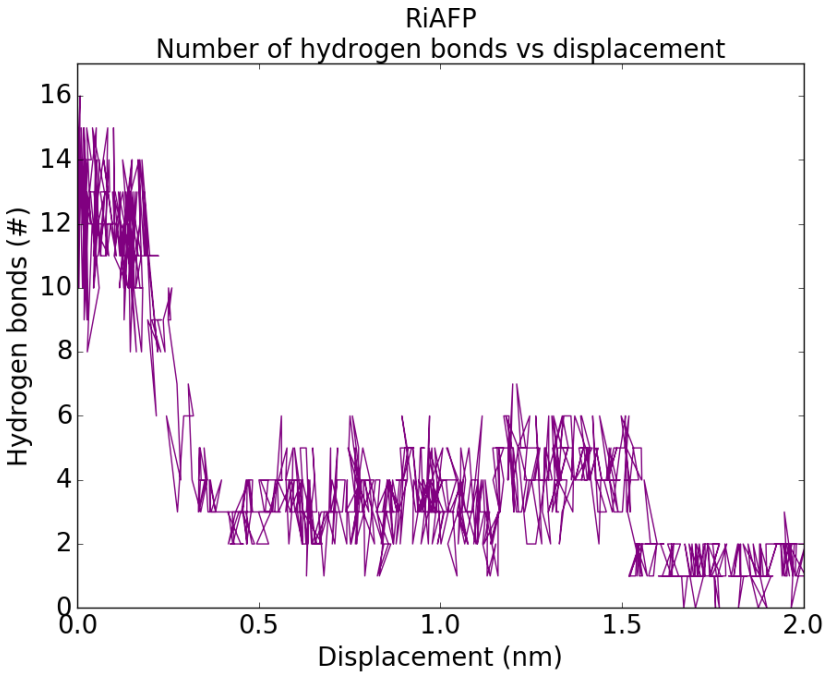

Figure 4: Number of hydrogen bonds between the turn being pulled and the adjacent turn versus the displacement of the pulled turn is plotted for RiAFP. This data is from one pulling simulation at 1 m/s, but is representative of all simulations.

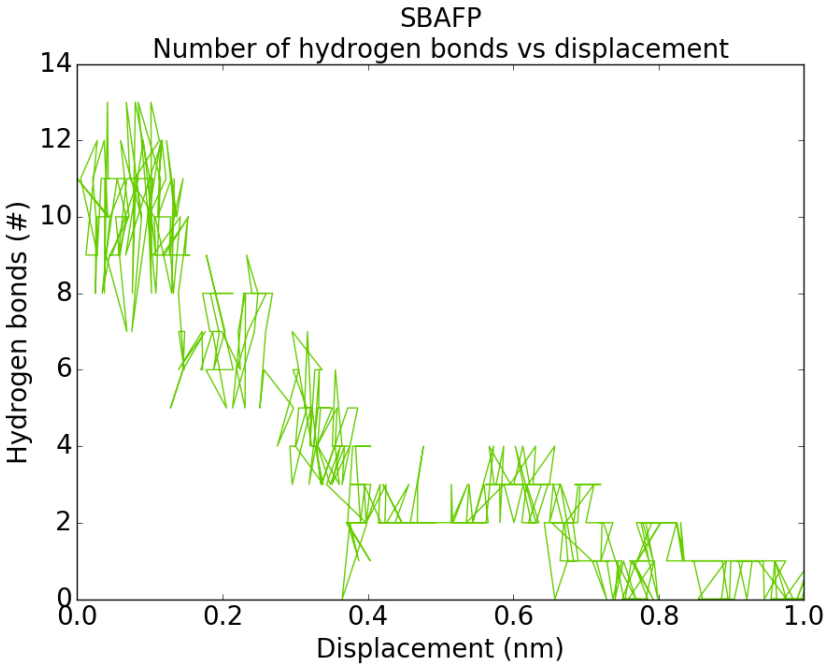

Figure 5: Number of hydrogen bonds between the turn being pulled and the adjacent turn versus the displacement of the pulled turn is plotted for SBAFP. This data is from one pulling simulation at 1 m/s, but is representative of all simulations.

Examples of this analysis are shown in Fig. 4 and Fig. 5. These figures show, on the y-axis, the number of hydrogen bonds between the pulled turn of the protein and the turn adjacent to it, during one pulling simulation done at 1 m/s. On the x-axis, is the displacement of the protein, analogous to what is shown on the x-axes in the plots in Fig. 7 of the main paper.

These plots show that before about 0.2 nm of displacement, the numbers of hydrogen bonds between the pulled turn and its neighbor fluctuates around a constant value (approximately 13 hydrogen bonds for RiAFP and 11 for SBAFP). At about 0.2 nm of displacement, there is a sharp drop in the number of hydrogen bonds for both proteins and this number continues to decline as the simulation continues. These results are consistent with the peaks of the force vs. displacement plots in Fig. 7 of the main paper, which occur at approximately the same displacement values.

Calculation of the number of hydrogen bonds between turns was done using the "gmx energy" tool in GROMACS [2].

7 Comparison to previous experimental and theoretical results for amyloids

Table 3 compares our results from theory and experiment to a range of other results for amyloid fibrils from other theoretical and experimental research. Note that the Young's modulus, experimentally, is ordinarily derived from an AFM based deflection method [1], while UTS is typically derived from sonication experiments like the one here. It is apparent that the values obtained in our work are well within the ranges of experimental and/or theoretical values from the literature.

Fibril	$Y_{exp}(GPa)$	$Y_{th}(GPa)$	$UTS_{exp}(GPa))$	$UTS_{th}(GPa)$	References
Modified SBAFP		11.0	0.66	0.31	This Paper
Modified RiAFP		7.9	1.6-5.5	0.38	This Paper
PrP	0.09	2.1/3.3	0.07	0.15/0.2	Lamour *et al.* [6]
Insulin	2.1	3.3	0.5	0.4	Lamour *et al.* [6]
Insulin	3.2				Adamcik *et al.* [1]
Insulin			0.7		Huang *et al.* [3]
Het-S	10.0	15.0	2.0	0.7	Lamour *et al.* [6]
Het-S		9.8		0.92	Solar & Buehler [10]
A-beta(1-42)		4.5		0.33	Lamour *et al.* [6]
A-beta(1-42)	3.2				Adamcik *et al.* [1]
A-beta(1-42)	1.79	4.5-38.0			Paul *et al.* [8]
A-beta(1-42)	3.2				Ruggeri *et al.* [9]
A-beta(1-40)		13.0		0.24	Solar & Buehler [10]
A-beta(1-40)$_{mut}$		11.7		0.4	Solar & Buehler [10]
α-Synuclein	2.2				Adamcik *et al.* [1]
α-Synuclein (ellip.)	0.08-0.17				Makky *et al.* [7]
α-Synuclein (tape)	0.15-0.3				Makky *et al.* [7]
β-Lactoglobin	3.7				Adamcik *et al.* [1]
Lysozyme	2.8				Adamcik *et al.* [1]
BSA	3.0				Adamcik *et al.* [1]
Ovalbumin	2.7				Adamcik *et al.* [1]
Tau	3.4				Adamcik *et al.* [1]
YadA CBP		12.6		0.55	Solar & Buehler [10]
LblBP		26.9		.69	Solar & Buehler [10]
GlmU		23.3		.63	Solar & Buehler [10]

Table 3: Selected Summary of Young's modulus and Ultimate Tensile Strength data from the amyloid literature

References

[1] J. Adamcik, C. Lara, I. Usov, J. S. Jeong, F. S. Ruggeri, G. Dietler, H. A. Lashuel, I. W. Hamley, and R. Mezzenga. Measurement of intrinsic properties of amyloid fibrils by the peak force qnm method. *Nanoscale*, 4(15):4426–4429, 2012.

[2] B Hess, C Kutzner, D van der Spoel, and E Lindahl. Gromacs 4: Algorithms for highly efficient load-balanced, and scalable molecular simulation. *J. Chem. Theory comput.*, (4):435–447, 2008.

[3] Yan Yi Huang, Tuomas P J Knowles, and Eugene M Terentjev. Strength of nanotubes, filaments, and nanowires from sonication-induced scission. *Advanced Materials*, 21:3945–3948, 2009.

[4] W Humphrey, A Dalke, and K Schulten. Vmd-visual molecular dynamics. *J. Molec. Graphics*, 14:33–38, 1996.

[5] E Krieger and G Vriend. Yasara view - molecular graphics for all devices - from smartphones to workstations. *Bioinformatics*, 30:2981–2982, 2014.

[6] G. Lamour, R. Nassar, P. H. W. Chan, G. Bozkurt, J. X. Li, J. M. Bui, C. K. Yip, T. Mayor, H. B. Li, H. Wu, and J. A. Gsponer. Mapping the broad structural and mechanical properties of amyloid fibrils. *Biophysical Journal*, 112(4):584–594, 2017.

[7] A. Makky, L. Bousset, J. Polesel-Maris, and R. Melki. Nanomechanical properties of distinct fibrillar polymorphs of the protein alpha-synuclein. *Scientific Reports*, 6, 2016.

[8] T. J. Paul, Z. Hoffmann, C. Z. Wang, M. Shanmugasundaram, J. DeJoannis, A. Shekhtman, I. K. Lednev, V. K. Yadavalli, and R. Prabhakar. Structural and mechanical properties of amyloid beta fibrils: A combined experimental and theoretical approach. *Journal of Physical Chemistry Letters*, 7(14):2758–2764, 2016.

[9] F. S. Ruggeri, J. Adamcik, J. S. Jeong, H. A. Lashuel, R. Mezzenga, and G. Dietler. Influence of the beta-sheet content on the mechanical properties of aggregates during amyloid fibrillization. *Angewandte Chemie-International Edition*, 54(8):2462–2466, 2015.

[10] M. Solar and M.J. Buehler. Tensile deformation and failure of amyloid and amyloid-like protein fibrils. *Nanotechnology*, 25(10), 2014.